In: Strontium Titanate
Editors: A. Tkach and P. Vilarinho

ISBN: 978-1-53615-437-5

Chapter 3

SR/TI RATIO IN STRONTIUM TITANATE CERAMICS: DESIGNING THE MICROSTRUCTURE, ENVISAGING THE PROPERTIES

***Luís Amaral*[1], *Alexander Tkach*[2], *Paula M. Vilarinho*[2,*]**
***and Ana M. R. Senos*[2]**
[1]Centre of Physics and Engineering of Advanced Materials (CeFEMA),
Instituto Superior Técnico, University of Lisbon, Lisbon, Portugal
[2]CICECO – Aveiro Institute of Materials, Department of Materials and
Ceramic Engineering, University of Aveiro, Aveiro, Portugal

ABSTRACT

Among the lead-free titanate-based materials, strontium titanate ($SrTiO_3$), pure or modified, is of particular importance. $SrTiO_3$ is an incipient ferroelectric with high dielectric permittivity and low losses, which finds application in tunable microwave devices due to a dependence

---

[*] Corresponding Author’s E-mail: paula.vilarinho@ua.pt.

of the permittivity on the electric field, or in grain-boundary barrier layer capacitors, taking advantage of highly resistive grain boundaries. The grain boundary characteristics and, therefore, electrical properties of polycrystalline $SrTiO_3$ are dependent on the defect chemistry and microstructure, which are thus fundamental in establishing the utility and value of the material. In their turn, such factors as Sr/Ti ratio, second phases or sintering conditions strongly affect the microstructure and alter the defect chemistry. Therefore, if properly understood these factors may be intentionally used to tailor the electrical response of electroceramics.

Starting from discovery of the grain growth anomaly in Ti-rich strontium titanate ceramics, impedance spectroscopy became a very useful tool in the investigation of this phenomenon, in addition to traditional defect chemistry and grain growth analysis. Three discontinuities in the Arrhenius-type temperature dependence of grain growth, which take place at sintering temperatures around 1500, 1550 and 1605°C, are accompanied by discontinuities in the dependence of the activation energy for grain boundary conductivity, which can be eliminated by annealing in oxygen. These results will be discussed briefly in the introductory section. This section of the chapter will be completed by a summary of an impedance spectroscopy study of $SrTiO_3$ ceramics with different Sr/Ti ratios (from 0.995 to 1.02). Bulk and grain boundary conductivity, activation energy and capacitance reveal strong systematic variations with the degree of nonstoichiometry. In the experimental results section of the chapter the effect of nonstoichiometry on the grain growth of $SrTiO_3$ ceramics is discussed. The grain boundary mobility assessed from grain growth data at 1450°C for Ti-rich, stoichiometric and Sr-rich compositions increases with decrease of the Sr/Ti ratio. An exponential increase of the grain boundary mobility with the grain size is also found independently of the Sr/Ti ratio, being more pronounced for the Ti-rich composition.

Keywords: nonstoichiometry, grain growth, grain boundaries, impedance spectroscopy, electrical properties

INTRODUCTION

Strontium titanate ($SrTiO_3$, STO) has been attracting a considerable interest from the fundamental point of view for a long time, often being used as a model system. STO is a quantum paraelectric [1], in which the dielectric permittivity monotonously increases upon cooling down to near 0 K, and no ferroelectric-type anomaly is observed due to quantum fluctuations. The low-temperature paraelectric phase is thus unstable, and the ferroelectric state can be induced in STO by the application of a high electric field [2], uniaxial stress [3], oxygen isotope exchange [4] or chemical substitutions in the lattice [5]. In addition, the dielectric permittivity of STO reveals a dependence on the applied bias electric field, called tunability and used in tunable microwave devices [6, 7]. Besides quantum paraelectric behaviour, interesting properties of STO include a structural phase transition [8], semiconductivity [9], superconductivity [10], and thermoelectricity [11], among others. Because of these properties, as well as good temperature and applied voltage stability at elevated temperatures, STO has been widely used in various grain boundary layer capacitors [12, 13] and varistors [14, 15]. The electrical properties of grain boundaries in STO, and their differences to the bulk, play a critical role in these devices [16]. For these applications, the material is usually heat-treated in a reducing atmosphere and with a donor addition to build a microstructure of semiconducting grains separated by insulating grain boundaries [12, 13]. Other potential application fields for STO range from high-density non-volatile memories [17, 18] or gate dielectrics in metal oxide semiconductor field effect transistor (MOSFET) devices [19], to sensors [20] or solid oxide fuel cells (SOFC) anodes [21].

Crystal Structure and Defect Chemistry of $SrTiO_3$

STO belongs to a class of ternary oxides, exhibiting a crystallographic structure related to that of calcium titanate ($CaTiO_3$) or perovskite. This family of oxides with perovskite structure is represented by the general formula ABO_3 and has a cubic unit cell, where A-cations are placed at the cube corners, small B-cations are located at the body centre position and oxygen ions (O^{2-}) at the centre of the faces [22], as schematically represented in Figure 1. The structure can also be regarded as a three-dimensional framework of BO_6 octahedra, arranged in a simple cubic pattern. In the octahedron unit, the B-atom is at the centre with the oxygen atoms at the corners shared by different octahedra and A-cations occupying the interstitial positions between the octahedra [22]. A-cations are 12-

coordinated and B-cations are 6-coordinated, and the ideal perovskite unit cell contains one formula unit, i.e., one A-cation, one B-cation and three oxygen ions.

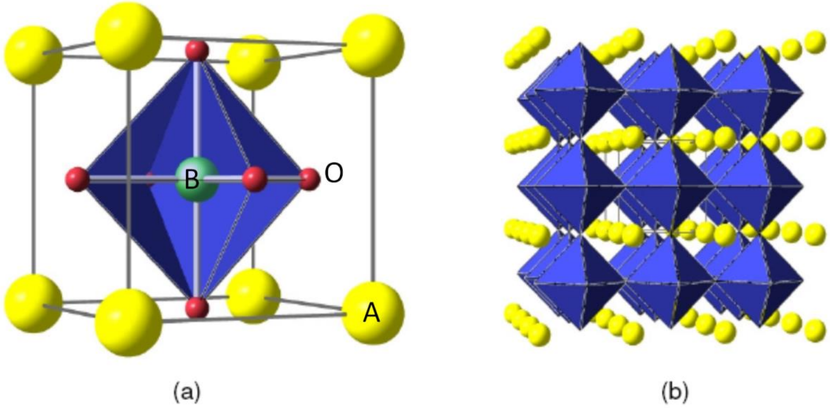

Figure 1. Two representations of the ideal cubic perovskite structure: (a) the cubic unit cell with octahedral coordination of the B-cation and (b) a corner sharing array of BO_6 octahedra.

A measure of the perovskite structure's stability is the Goldschmidt tolerance factor [23, 24], t_G, that relates the ionic radii of the constituents of the perovskite lattice:

$$t_G = \frac{r_A + r_O}{\sqrt{2}(r_B + r_O)} \quad (1)$$

where r_i (i = A, B, O) denotes the average ionic radii of the constituents of the ABO_3 compound in the respective sites. The tolerance factor is also a measure of the deviation from the ideal packing while maintaining a stable perovskite structure. For $t_G < 1$, the size of the unit cell is governed by the B-site ion and the A-site ions are allowed to fluctuate in their sites. For $t_G > 1$, the B-site ions have too much space to vibrate whereas the A-site ions are closely packed. For $t_G = 1$, both A and B ions are closely packed.

STO is considered an example of the ideal cubic perovskite structure [8]. In STO, A-sites are occupied by Sr^{2+} ions and B-sites by Ti^{4+} ions. At room temperature, STO has an undistorted cubic perovskite structure of the space group Pm3m and its lattice constant is 3.905 Å [24, 25]. STO presents a phase transition from cubic to tetragonal phase (space group I4/mcm) around 105-110 K [8, 26], related with tilting of the oxygen octahedra around one of the [100] axes [27]. Therefore, the tetragonal phase is centrosymmetric and no polarization is induced in STO below the transition temperature.

The tolerance factor for STO is $t_G \approx 1$ [4], implying a high (ideal) packing degree. Therefore, it is generally accepted that interstitial occupation is not likely in STO [4]. Moreover, the solubility limits for either Sr- or Ti-excess in the STO lattice are quite low, as has been discussed for decades [28, 29, 30, 31]. Nevertheless, some incorporation is still possible [32]. Titanium vacancies are generally considered unlikely defects because of its high effective charge that corresponds to a major disruption of the chemical bonding of the crystal. On the other hand, theoretical calculations within STO defect models indicate that vacancy disorder is predominant in this material [33]. Accordingly, oxygen vacancies are known to be easily formed in perovskite compounds [29, 34], and strontium vacancies are often assumed to be the most important defect compensation mechanism in STO [33, 35, 36, 37, 38, 39].

Table 1. Possible incorporation mechanisms of excess oxide, SrO or TiO$_2$ in STO

Incorporation mechanism	Eq.	Refs.
SrO-excess		
$SrO \rightarrow Sr_{Sr} + V_{Ti}^{''''} + O_O + 2V_O^{\bullet\bullet}$	(2)	[28, 29, 32]
$2SrO \rightarrow Sr_{Sr} + Sr_{Ti}^{''} + 2O_O + V_O^{\bullet\bullet}$	(3)	[28, 29]
TiO$_2$-excess		
$TiO_2 \rightarrow V_{Sr}^{''} + Ti_{Ti} + 2O_O + V_O^{\bullet\bullet}$	(4)	[28, 29, 32, 40]

After these considerations, excess oxide, SrO or TiO$_2$ may be incorporated in the perovskite lattice as shown in Table 1 and described in the following text. The incorporation of SrO-excess requires the formation of interstitial strontium and oxygen, which are not likely and therefore neglected, or titanium and oxygen vacancies [28, 29, 32] according to Eq. (2). However, considering the high charge of titanium vacancies, the incorporation of Sr-excess would not be very favourable. On the other hand, part of the Sr^{2+} ions can occupy B sites as presented in Eq. (3) and was observed in some perovskite related compounds [28, 29], not allowing to one exclude this form of SrO-excess incorporation.

According to Witek et al. [28], the solubility limit of SrO-excess does not extend beyond Sr/Ti = 1.002. Nevertheless, SrO-excess is known to accommodate in the STO lattice as a three-dimensional mosaic of single-layered rock-salt blocks, forming the so-called Ruddlesden–Popper structures with the formula $SrO{\cdot}(SrTiO_3)_n$ [29, 32, 40, 41].

On the other hand, neglecting interstitial occupation, the incorporation of TiO_2-excess into the lattice requires the formation of strontium and oxygen vacancies [28, 29, 32, 40] according to Eq. (4). As mentioned above, the ease of formation of oxygen vacancies in perovskite compounds, and the fact that strontium vacancies are assumed to be the most important compensation mechanism in STO [33, 35, 36, 37, 38, 39], support this model as the way of incorporating TiO_2-excess. The presence of TiO_2 (rutile) as a second phase [28, 42] was reported for STO with TiO_2-excess of 0.5 mol% (Sr/Ti = 0.995).

Point defect models discussed above for STO assume that the material is a homogeneous and isotropic system with a diluted concentration of defects. However, grain boundaries are present in polycrystalline materials and greatly affect the local defect chemistry and, thereby, the overall microstructural evolution and electrical behaviour of ceramics. Moreover, defects may be directly related to the structure of grain boundaries. For example, Chung et al. [35] reported that high ionic vacancy concentration can induce interface roughening in STO.

On the other hand, charge transport in a heterogeneous material may involve bulk pathways and transport across boundaries as well as along boundaries. The behaviour of the material, therefore, turns out to depend significantly on the properties of the grain boundaries, which are markedly affected by its defect chemistry, rather than on the properties of the bulk grains [35, 43, 44]. In fact, as previously mentioned, some electrical properties required for particular applications, such as boundary layer capacitors, low-voltage varistors, or positive temperature coefficient thermistors, are a consequence of highly engineered grain boundary electrical barriers [45]. In these cases, grain boundaries are often affected by depletion effects, and exhibit highly resistive behaviour [16, 45, 46] acting as barriers to the transport of charge carriers. The basis for the formation of a charged surface or grain boundary in ionic solids is the difference in the individual defect formation energies [45].

For undoped and acceptor-doped alkaline earth titanates, positively charged grain boundary interface states seem to be active even at sintering temperatures [45]. A space charge layer model was developed for grain boundaries in acceptor-doped titanate ceramics, which is valid for nominally undoped materials as well due to uncontrolled impurities [45, 46, 47, 48]. Due to the existence of positively charged grain boundary states, the regions close to the grain boundaries are depleted of mobile charge carriers with the same charge sign as the grain boundary states (oxygen vacancies and holes are repelled from the vicinity of the grain boundary). At the same time, electrons are accumulated because the positive grain boundary charge has to be compensated by a negative space charge on both sides of the grain boundary built up by the immobile bulk acceptors.

This redistribution of charges leads to the formation of the space charge layer. The grain boundary resistivity can be explained by the fact that the major charge carriers have to overcome this positively charged barrier. The width of the grain boundary depletion layer in acceptor-doped STO has been determined to be 30-200 nm, decreasing with increasing acceptor concentration [46].

The structural accommodation between two grains occurs approximately over only a few nm [44]. The investigations of the grain boundary region in $BaTiO_3$ and STO by Chiang and Takagi revealed a strong segregation of acceptor impurities at the grain boundary [45, 47]. In contrast, a segregation of donors was not observed. However, another study revealed slight donor segregation [44] at the grain boundaries in polycrystalline STO. Chiang and Takagi also found Ti in excess at the grain boundaries and no systematic variation in the excess of Ti with the overall composition, including A site/B site cation stoichiometry [45].

Other investigations confirm the presence of Ti-rich layers at grain boundaries [34, 49, 50]. Oxygen deficiency at the interfaces due to unoccupied lattice sites and oxygen vacancy segregation at the boundary has also been reported [49]. These vacancies are compensated by electrons resulting from the lowering of the Ti valence, which form an *n*-type layer at the interface.

More recently, Bäurer et al. [51], using scanning transmission electron microscopy (STEM) coupled with energy dispersive spectroscopy (EDS), observed local nonstoichiometry at the grain boundaries of strontium titanate as well. Ti-rich, neutral and Sr-rich grain boundaries were detected, independently of the bulk composition (Ti or Sr- rich) [51]. This indicates that grain boundaries bring additional degree of freedom in a phase diagram, where compositions not stable as a bulk phase are possible. Ti-rich boundaries showed a retarding effect on grain boundary mobility, probably due to a solute drag mechanism. On the other hand, long (100)-facets, which were neutral or Sr-rich, showed the highest mobility [51]. This was correlated to the high number of Ti and O vacancies in these grain boundaries [52, 53]. It is important to note here that the nonstoichiometry at the grain boundaries must be compensated by defects accommodating the excess of the other species in the bulk. Ti or Sr-excess accommodation will be reviewed ahead.

Grain Growth and Grain Boundary Phenomena in $SrTiO_3$

Grain growth in titanates is very complex and generally depends on many factors such as oxygen partial pressure, dopant species and concentration, nonstoichiometry and sintering temperature, among others, which affect the grain boundary characteristics. All these factors are important to understand the microstructure evolution of titanates during sintering. In this way, if understood and controlled, they may be used to obtain the desired final microstructures.

The grain growth of STO has fundamentally and technologically interested researchers for a long time, and new revealing results have been published in recent years [54]. Particular attention has been given to grain boundaries and their relationship with the grain growth of STO. The main observations are summarised in the following text.

Related to high interface anisotropy, the faceting of grain boundaries of STO has been related to the origin of abnormal grain growth [55]. Due to a nucleation energy barrier for new atomic layers on a singular surface, some grains may grow abnormally if favoured by the existence of attachment sites [56], such as dislocations [57]. This nucleation-limited growth theory was experimentally validated for STO grain coarsening in a Ti-rich liquid [35, 56]. The phase diagram of the SrO-TiO_2 system has the eutectic point at about 1440°C for Ti-rich compositions [58]. When a nonstoichiometric ceramic with Sr/Ti < 1 is sintered above this temperature, a Ti-rich liquid phase forms and affects the densification and grain growth of this material. In the case of the Sr-excess side of the diagram, the eutectic is at 1830°C, far above the generally used sintering temperatures.

Accordingly, Chung and Kang [57, 59] showed that dislocations enhance the mobility of faceted flat interfaces in the presence of a thin liquid film between grains in STO. Dislocations did not play any role on grain growth promotion when the interfaces were curved. Additionally, the effect of dislocations occurred only when the grain boundaries were wetted by an intergranular amorphous phase [59]. From these observations, the authors suggested that an uneven distribution of dislocations might be a cause of abnormal grain growth in polycrystalline STO.

Lee et al. [60] used high-resolution electron microscopy to investigate the temperature dependence of faceting of an asymmetric boundary between two STO crystals in the temperature range of 1100 to 1600°C. The boundary was faceted with changes in facet symmetry occurring at 1300°C. At 1600°C, faceting disappeared and the grain boundary became defaceted, indicating the occurrence of a grain boundary faceting-defaceting transition [60]. In a related investigation [61], the authors observed that the defaceting transition occurred suddenly between 1570 and 1590°C.

Further developments were made using a combination of impedance spectroscopy (IS), high resolution TEM (HRTEM) and electron energy loss spectroscopy (EELS). The rough grain boundary observed at 1600°C contained more oxygen vacancies than the faceted grain boundaries observed below 1600°C [62]. Moreover, the disordering of the grain boundary by the defaceting transition caused an abrupt appearance of grain-boundary impedance at 1600°C in Nyquist diagram, demonstrating a relation between the change in grain boundary impedance, grain boundary electronic structure and the grain boundary faceting-defaceting transition [62].

The presence of an intergranular glassy film (IGF) has a significant effect on the grain growth of STO [59, 63]. The distribution of such amorphous phases is important and may change considerably, depending on the annealing path and conditions [59]. In Ti-excess STO with a low donor concentration, a continuous liquid film wets the grain boundaries and faster grain growth occurs [63]. It was also reported that in the presence of a thin liquid film between grains, dislocations promote the grain growth of STO [57, 59]. In another work, 1 mol% TiO_2 was added to STO powders to create a TiO_2-excess liquid above the eutectic temperature [35]. TEM showed a liquid phase in the triple junction of the grains, and the interface between the STO grains and the liquid was faceted [35].

Thus, nonstoichiometry is an important aspect influencing grain growth in titanates, and particularly in STO. It is often found that TiO_2-excess improves densification while SrO-excess deteriorates it, as observed by Chen et al. [64]. A strong influence of nonstoichiometry on the densification of STO was observed in dilatometric experiments [32, 42] with higher densification rates measured for Ti-rich compositions [32]. In fact, our previous studies revealed two peaks in the dependence of the densification rate on the temperature for stoichiometric and Ti-rich samples (more pronounced in the latter case), whereas a single mode curve characterised the Sr-rich composition [32]. The position of the peaks varied systematically with the Sr/Ti ratio and was below the eutectic temperature; this might be related to the formation of IGFs, leading to subsolidus activated sintering, as previously discussed.

The densification behaviour of stoichiometric compositions is usually closer to that of Ti-rich compositions than to that of Sr-excess ones [32, 42]. Additionally, coarser-grained microstructures and higher grain growth rates are observed with the decrease of the Sr/Ti ratio [32, 64, 65, 66]. Sr-excess normally leads to normal grain growth, whereas abnormal grain growth is often observed for Ti-rich compositions [64, 67].

The changes in the sintering behaviour of STO induced by nonstoichiometry have been correlated with changes in the defect chemistry of the material introduced by the incorporation of the excess oxide [32, 42], as previously discussed. It is also important to recall that, although the liquid phase may form above 1440°C for Ti-excess STO compositions, enhancing matter transport, abnormal grain growth in STO without detected liquid phase has also been reported [51, 68].

Thus, recent grain growth studies of nonstoichiometric STO ceramics sintered in an oxygen atmosphere from 1425 to 1600°C [51] reported that both Ti-rich (Sr/Ti = 0.996) and Sr-rich (Sr/Ti = 1.002) compositions show the same overall grain growth behaviour, with abnormal grain growth being observed in both cases. On the other hand, in a composition with higher SrO excess, Sr/Ti = 1.005, grains grew normally but with a grain boundary mobility that was similar to the mobility of the abnormal grain growth of the other compositions.

A deeper correlation between grain growth behaviour and grain boundaries in STO was attempted using HRTEM and STEM-EDS. Grain boundaries of normal and abnormal grains were investigated [51]. Four types of grain boundaries were reported. Type A grain boundaries were atomically flat with a boundary plane parallel to the (100) plane in one of the adjacent grains; type B had the same boundary plane orientation but were atomically disordered or rough; type C were stepped boundaries and type D boundaries were curved. Grain boundaries of types C and D did not show a preferred crystallographic orientation of the grain boundary plane for either of the adjacent grains [51].

The grain boundary chemistry was also evaluated and nonstoichiometry at the grain boundaries was found, weakly correlated to boundary morphology [51]. Ti-rich, neutral and Sr-rich grain boundaries were detected, independently of the bulk composition. The boundary chemistry showed an important effect on the boundary kinetics, with neutral or Sr-rich (100)-faceted boundaries showing the highest mobility. On the other hand, Ti-rich boundaries revealed a retarding effect on grain boundary mobility, which was attributed to a solute drag mechanism [51]. Sr-rich boundaries were only detected in the types A and B, whereas no Ti-rich type A boundary was observed. Additionally, type A boundaries were not detected in Sr/Ti = 1.005 that did not show abnormal grain growth. In agreement, abnormal grains in the Sr/Ti = 0.996 composition exhibited the largest fraction of this type of boundary and only a small fraction of type D ones. In the Sr/Ti = 1.005 composition, type B boundaries were the largest fraction. On the other hand, the normally grown grains of the Ti-rich composition had more similar fractions of all four kinds of boundaries.

The grain boundary types observed in STO were correlated to the boundary complexions defined in alumina doped with silica or calcia by Harmer and co-workers [69, 70, 71]. By intensive grain growth studies in alumina, six different types of kinetic behaviour were identified and each of them was associated with a grain boundary structure or “phase”, which was called complexion [69]. Complexion I is related to sub-monolayer adsorption in the boundary core of dopant cations that results in solute drag. Complexion II shows no segregation, is a ‘‘clean’’ grain boundary of undoped alumina. Complexion III consists of bilayer adsorption that enhances grain boundary mobility relative to undoped alumina. Complexion IV contains a disordered layer that is associated with multilayer adsorption. The mobility of these grain boundaries is about one order of magnitude higher than that of clean grain boundaries. Complexion V is associated with a thin equilibrium thickness amorphous intergranular film, often referred as intergranular glassy film. This interface has typical grain boundary mobilities that are a factor of 50 faster than those for normal grain growth in undoped alumina. Finally, complexion VI is associated with a wetting grain boundary film. This complexion has a mobility that is over two orders of magnitude larger than that of undoped alumina.

Thus, in STO the low-mobility Ti-excess boundaries were compared to complexion I where the movement is retarded by segregation of species. The stoichiometric boundaries were found to be of type II, whereas high-mobility nonstoichiometric boundaries were associated with complexion III [51]. However, Bäurer et al. [51] did not report any amorphous films at the grain boundaries for either normal or abnormal grains, which would be essential for the formation of complexions of types IV to VI, as observed by Dillon et al. [69]. Nevertheless, it should be possible to induce these complexions in STO by the stabilisation of a liquid film at the grain boundaries, leading to higher grain boundary mobilities [51]. According to Bäurer et al. [51], the observation of the different grain boundary types in STO is in agreement with the explanation of abnormal grain growth by the co-existence of two or more grain boundary complexions [69], with the correspondent differences in mobility.

In a related investigation, a grain growth anomaly in STO was observed [72]. Bäurer et al. studied the grain growth behaviour of STO sintered in oxygen in the temperature range of 1200 to 1600°C. They reported two drops in the grain boundary mobility with increasing temperature, independent of the A-site to B-site stoichiometry. The grain growth kinetics did not follow the classical Arrhenius-type temperature dependence, indicating changes in the basic mechanism of grain boundary motion [72].

The unexpected grain growth behaviour observed in STO was related to structural changes of the grain boundaries at high temperatures, such as changes in the faceting behaviour [52, 72]. In samples sintered at 1425°C, a high preference for grain boundary planes oriented parallel to the [100] direction of one of the adjacent grains was found [51], which did not exist in the lower temperature regime (samples sintered at 1300°C) [52]. This was pointed out as a possible explanation for the change in grain growth rate [52].

Discontinuities in the evolution of grain growth with the sintering temperature were also reported by some of us in a 0.5 mol% Ti-rich STO composition (Sr/Ti = 0.995), and we have defined four grain growth regimens with transitions at temperatures around 1500, 1550 and 1605°C [73]. These transitions correspond to grain size decreases, despite the increasing sintering temperature, as shown in Figure 2. Moreover, this anomalous behaviour is directly related to the presence of a liquid phase, the amount of which varies discontinuously with the temperature. A first order reverse change of complexions driven by the temperature effect on the grain boundary wettability and electrostatic potential was suggested to explain these anomalies.

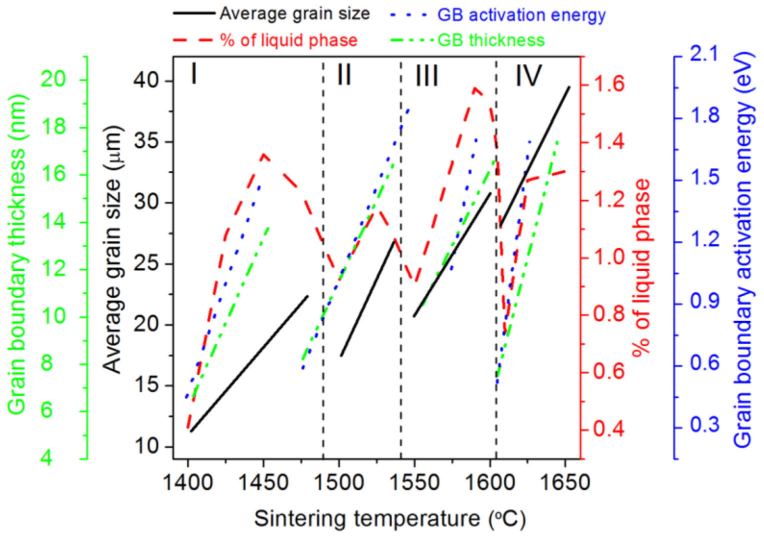

Figure 2. Illustration of the dependence of the average grain size (solid lines), percentage of liquid phase (dashed lines), activation energy for grain boundary conductivity (dotted lines) and grain boundary thickness (dash-dot lines) on the sintering temperature (adapted from Ref. [73]). There is a clear relation between all these parameters, unambiguously defining four regimens.

Effects on the electrical properties were also verified by IS. The correlation between discontinuities in grain growth behaviour and grain boundary electrical response was observed for the first time [73]. Grain boundary electrical response was much more affected by the sintering temperature than that of the bulk counterpart. Furthermore, changes were detected in the activation energy for grain boundary conductivity and grain boundary thickness, as also seen in Figure 2, in correlation to the formation of an amorphous phase and to the grain growth regimens detected by scanning electron microscopy (SEM) [73]. A levelling-off in the grain boundary conductivity activation energy, which increases for up to 1.2 eV, and a four-fold decrease in the grain boundary permittivity, were observed after annealing these ceramics in oxygen atmosphere, thus, confirming a key role of oxygen vacancies in the relation between the grain growth and grain boundary conductivity anomalies of as-sintered Ti-rich STO ceramics [74].

The effect of nonstoichiometry (Sr/Ti ratio from 0.995 to 1.02) on bulk and grain boundary contributions to the electrical response of STO ceramics was also systematically investigated by us, and compared with the microstructure development [75]. With the exception of the highest Ti excess, the grain size distribution was enlarged and grain size increased with the decrease of the Sr/Ti ratio. However, IS, being a very sensitive and powerful technique for the study of the effect of small stoichiometric variations, revealed that the resistivity of bulk and grain boundaries systematically decreased in both Ti-rich and Sr-rich STO as compared to stoichiometric ceramics. The effect is much stronger for the grain boundaries as compared to the bulk. Therefore, it was suggested that defect chemistry plays a much more important role in the electrical response of STO than microstructural development [75]. Indeed, very small variations in the stoichiometry induce a high number of defects, in which ionisation increases the charge carrier concentration, leading to a strong reduction of the resistivity, particularly at the grain boundaries.

Moreover, systematic dependences on the nonstoichiometry were also observed for the conductivity activation energy and capacitance (much more affected in the case of the grain boundary rather than the bulk contribution) [75]. These observations are also consistent with the strong impact of nonstoichiometry induced defect chemistry and correspondent modification of grain boundary complexions, which lead to different microstructure evolution and diverse electrical responses. Thus, nonstoichiometry enables the design of the electrical properties and grain boundary engineering of ceramics.

Hence, although only in collaboration with defect chemistry, microstructure engineering can help to anticipate the electrical and other properties of STO. Therefore, a study of the effect of nonstoichiometry on grain growth, particularly the grain boundary mobility, of STO ceramics sintered at 1450°C is presented here.

METHODS

Ceramics of STO compositions with Sr/Ti ratios of 0.995, 1.000, and 1.020 (hereafter named as ST 0.995, ST, and ST 1.02, respectively) were prepared by conventional mixed oxide method. Raw powders of $SrCO_3$ and TiO_2 (pro analysis (purity $\geq$ 99%), Merck) were ball milled in alcohol in a planetary mill for 5 h, using Teflon pots with zirconia balls. After calcination, at 1100°C for 2 h, the powders were monophasic. Powders were then milled again under the same conditions, uniaxially pressed at 50 MPa and further isostatically pressed at 200 MPa.

Grain growth studies were performed at 1450°C with isothermal times from 0.1 to 12 h. Ti-rich ST 0.995 samples were heated up to the sintering temperature of 1450°C with a heating rate of 20°C/min. At the end of the isothermal sintering time, the samples were removed from the furnace. After sintering for 0.1 h ST 0.995 ceramics presented a relative density of 98 ± 1%. Stoichiometric (ST) and Sr-rich (ST 1.02) ceramics used in the grain growth studies at 1450°C were previously densified at 1350°C for 2 h. The attained relative density was 96 ± 1% in both cases. In order to eliminate the remaining porosity, the samples were then submitted to a step of hot isostatic pressing for 1 h at the same temperature of 1350°C and a pressure of 50 MPa. The hot-pressed samples were 99 ± 1% dense, close to full densification. The dense ceramics were then introduced into a tubular furnace at the intended temperature of 1450°C and annealed in air for several isothermal times. The equivalent high density of the different ceramic compositions is important for further comparison of grain growth data because it assures that all the ceramics had reduced pore restraining effects on coarsening.

Polished and thermally etched sections of the sintered ceramics were observed by SEM (Hitachi S-4100). Using ImageJ software, the grain size distribution of the sintered ceramics was determined, taking more than 600 grains in, at least, three SEM micrographs. The area of the section of the grains was measured and then its circular equivalent diameter calculated. The average grain size, G, was determined from the average equivalent diameter, by using a multiplying factor of 1.22. The error bars were derived from the standard deviation of the values measured in the different images.

RESULTS AND DISCUSSION

In spite of the stoichiometry variations between the compositions, the X-ray diffraction (XRD) patterns of the calcined powders showed the peaks consistent with the cubic perovskite crystallographic structure of STO in all cases [32]. No second phases were detected in any of the compositions, within the detection limit of the XRD technique. The particle size distribution of calcined powders analysed by laser diffraction (Coulter) has shown equivalent particle size and size distribution for all the compositions. A bimodal size distribution could be observed in all the cases, with peaks around 0.2 and 2-3 µm. The first peak of the distributions is always below 1 µm whereas the second one corresponds mainly to agglomerates in the powder suspensions that are destroyed after pressing [32].

Grain growth studies were performed, and grain boundary mobility was evaluated using ST 0.995 (Ti-rich), ST (stoichiometric) and ST 1.02 (Sr-rich) compositions. Figure 3 presents SEM micrographs of the stoichiometric and nonstoichiometric STO ceramics after the thermal treatment at 1450°C, for several isothermal times.

Coarsening of the microstructure with increasing isothermal time is observed for all the three compositions. Moreover, larger grain size is attained for the Ti-rich composition, ST 0.995 (with a lower magnification in Figure 3, left). Detailing these observations, the evolution with the isothermal time of the equivalent diameter (representing grain size) distribution and the average grain size obtained from these distributions are presented for the three compositions in Figure 4 and Figure 5, respectively. In agreement with previously reported results [32, 65], the enlargement of the grain size distribution and the increase of the attained grain size with the decrease of Sr/Ti ratio are clearly observed.

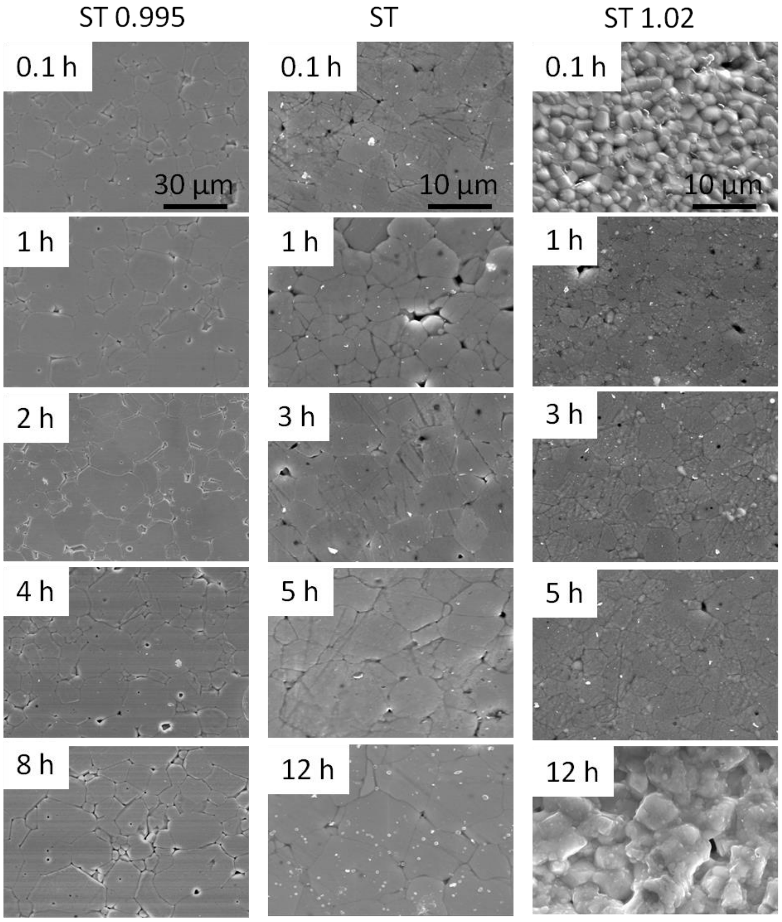

Figure 3. SEM micrographs of the three compositions: Ti-rich, ST 0.995 (left), stoichiometric, ST (middle) and Sr-rich, ST 1.02 (right) after thermal treatment at 1450°C for several periods. Coarsening of the microstructures is visible, as well as the increase of the attained grain size with the decrease of the Sr/Ti ratio.

Despite the effects of the nonstoichiometry on the grain size and grain size distribution, the data regarding the three compositions is consistent with a normal grain growth mode for all the cases under study. The grain growth data in Figure 5 was used to assess the effect of nonstoichiometry on the grain boundary mobility of STO. As previously mentioned, the grain boundary mobility, *M*, is the proportionality factor between the driving force for grain growth and the average grain boundary velocity [76, 77].

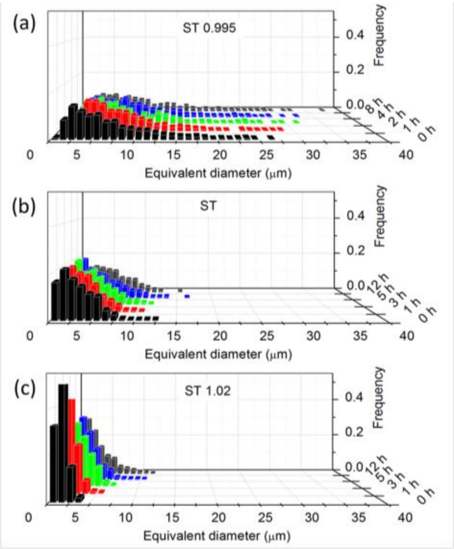

Figure 4. Equivalent diameter distribution evolution with the isothermal time at 1450°C for the three compositions: (a) Ti-rich ST 0.995, (b) stoichiometric ST and (c) Sr-rich ST 1.02. Larger grain size and enlargement of the grain size distribution are observed with the increase of the Ti content.

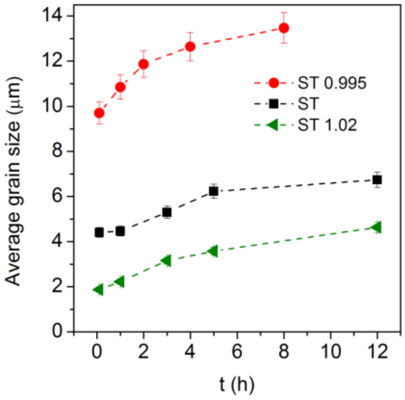

Figure 5. Average grain size evolution with the isothermal time at 1450°C for the Ti-rich (ST 0.995), stoichiometric (ST) and Sr-rich (ST 1.02) compositions. Along the entire sintering cycle, larger grain size is attained with the decrease of the Sr/Ti ratio.

The grain growth kinetics is typically described as [69, 76]:

$$G^m - G_0^m = k\Delta t \quad (5)$$

with G_0 the initial average grain size at the time t_0, G the average grain size at the time t, m the grain growth exponent and k the grain growth factor. In order to extract grain boundary mobilities from grain growth data, m must be assumed to be 2 (parabolic kinetics), implying a dense system with clean grain boundaries [69]. However, parabolic kinetics does not typically provide the best fit for normal grain growth data, since drag effects [78] normally cause the grain growth constant to be greater than two. In other words, the grain boundary mobility is not constant and decreases with increasing grain size due to the decrease of specific grain boundary area and a consequent increase of the impurity drag effect [69, 78].

Nevertheless, the decrease in mobility is typically small, and the exponent $m = 2$ was indeed shown to adequately fit the normal grain growth data [51, 69, 70, 71, 72]. In these conditions, the growth factor k is given by the following equation [76]:

$$k = 2\alpha\gamma M \tag{6}$$

where α stands for a geometrical factor of the order of the unit and γ for the grain boundary energy, which is not expected to vary significantly from grain boundary to grain boundary in most ceramics [69], and the possible changes in boundary energy are small compared to the overall changes in k [51].

The grain size $(G^2 - G_0^2)$ versus time at 1450°C for the three compositions, assuming parabolic kinetics, is presented in Figure 6 (a). According to Eq. (6), this plot yields a linear relation, as can be effectively observed. This means that parabolic kinetics provide a reasonable fit of the grain growth data. The growth factor k may then be extracted from the slope of the lines, and can be used as a comparable value for the "effective mobility" of the grain boundaries. However, for long sintering times, some deviation from linearity is observed. As previously mentioned, this may be related to increased impurity drag effects due to increasing grain size, and a consequent decrease of the grain boundary area [78].

The deviation from linearity, when long sintering times are considered, is almost negligible for the ST 1.02 composition, but significantly increases with increasing Ti content. This is seen when comparing the linear fits for data with (dashed lines) and without (solid lines) the longest heating periods in Figure 6 (a). Nevertheless, for short isothermal times, parabolic kinetics were revealed to fit the data adequately regarding the three compositions. In these conditions, the effect of possible impurities is lessened and the grain boundary mobility can be properly assessed. Therefore, the growth factor was calculated excluding the data corresponding to the longest isothermal times, as presented in Figure 6 (a) (solid lines). The results are presented in Figure 6 (b) plotting the dependence of the growth factor k on the Sr/Ti ratio. A marked increase of the growth factor with decreasing Sr/Ti ratio is clearly observed.

These observations of a strong dependence of the grain boundary mobility on the Sr/Ti ratio are in agreement with previous results on the effect of the nonstoichiometry on the densification kinetics of STO [32]. In that work, Ti excess (Sr/Ti = 0.997) enhanced matter transport during sintering, whereas Sr excess (Sr/Ti = 1.02) decreased it. However, the present findings differ from the results of Baürer et al. [51, 72], where no substantial differences in the effective mobility with the variation of the Sr/Ti ratio from 0.996 (Ti-excess) to 1.005 (Sr-excess) was observed. At the sintering temperature of 1450°C, the growth factor reported by Baürer et al. [51, 72] was around 4×10^{-17} m^2/s for normal grain growth in ceramics with Sr/Ti ratios of 0.996 and 1.002, while for abnormally grown grains it was around 1×10^{-15} m^2/s, this being the same as for normal grain growth of the Sr/Ti = 1.005 composition. The growth factor values obtained in the present work, and presented in Figure 6 (b), on average are closer to the later value (1×10^{-15} m^2/s). The growth factors found for the Ti-rich and stoichiometric compositions are higher than the referred-to value by factors of ~4 and 1.3, respectively, whereas the value for ST 1.02 is approximately half of that value.

Nonetheless, in addition to the differences in the Sr/Ti ratios used in the two works, the ceramics studied by Baürer et al. were sintered in an oxygen atmosphere [51, 72], which may have a strong impact in the sintering process. In fact, the different behaviours associated to different sintering atmospheres is a strong indication of the role of the defect chemistry alterations induced by the nonstoichiometry on the grain boundary properties. In particular, the oxygen vacancy concentration, which should be minimised in an oxygen atmosphere, may be an important factor in determining the grain boundary mobility in STO.

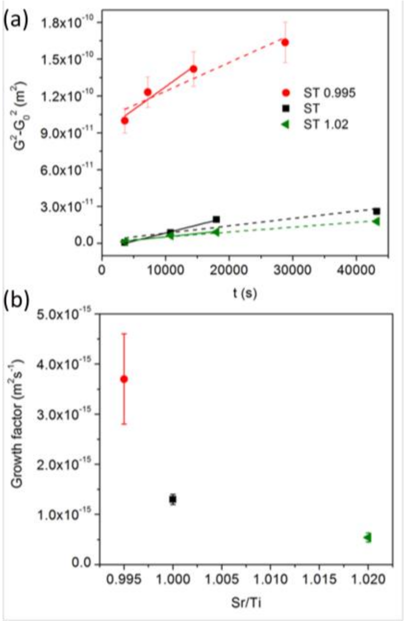

Figure 6. (a) Grain size versus time at 1450°C for the Ti-rich (ST 0.995), stoichiometric (ST) and Sr-rich (ST 1.02) compositions. Parabolic kinetics provides a good fit to the grain growth data of the three compositions for short sintering times. (b) Growth factor, k, at 1450°C for the Ti-rich (ST 0.995), stoichiometric (ST) and Sr-rich (ST 1.02) compositions. The growth factor increases significantly with the increase of the Ti content.

Another aspect to be considered in this discussion are the changes at grain boundaries induced by impurities, as reported before [63]. However, the STO compositions under study were prepared from the same reagents with only minor variations of the stoichiometric proportions. Therefore, the impurity content should be essentially the same for all the compositions. On the other hand, the effect of the same impurity content may depend on the Sr/Ti ratio, because impurities may have a higher affinity for either the A or the B site of the perovskite lattice. For example, Si impurities occupying the Ti site of the perovskite lattice are expelled from the crystal structure by Ti-excess [63]. Hence, the effect of impurities on changing the grain boundary properties may not be completely excluded.

CONCLUSION

The effect of nonstoichiometry (Sr/Ti ratio from 0.995 to 1.02) on the grain growth was presented and discussed. The grain boundary mobility assessed by extracting growth factors from grain growth data at 1450°C was found to increase with the decrease of the Sr/Ti ratio. The enlargement of the grain size distribution and the increase of the attained grain size with the decrease of Sr/Ti ratio were observed, thus, offering a tool for microstructure tailoring and grain boundary engineering of strontium titanate ceramics. However, this tool can be useful to envisage the properties only when relations between the defect chemistry and grain boundary phenomena, including grain boundary contributions to the electrical response of strontium titanate ceramics, reviewed in this chapter, are taken into account.

ACKNOWLEDGEMENTS

This work was developed within the scope of the project CICECO-Aveiro Institute of Materials, FCT Ref. UID/CTM/50011/2019, financed by national funds through the FCT/MCTES. The authors acknowledge as well the financial support from the Foundation for LusoAmerican Development (FLAD), Portugal. FCT is also acknowledged for financial support by Luís Amaral "(SFRH/BD/40927/2007, SFRH/BPD/97453/2013 and contract no. IST-ID/153/2018) and Alexander Tkach (IF/00602/2013). Thanks to Dr. R. C. Pullar who assisted with the English language of this chapter.

REFERENCES

[1] Müller, K. A., Burkard, H. 1979. "$SrTiO_3$ - An Intrinsic Quantum Paraelectric below 4K." *Phys. Rev. B* 19:3593-3602.

[2] Fleury, P. A., Worlock, J. M. 1968. "Electric-field-induced Raman Scattering in $SrTiO_3$ and $KTaO_3$." *Phys. Rev.* 174:613-623.

[3] Uwe, H., Sakudo, T. 1976. "Stress-induced Ferroelectricity and Soft Phonon Modes in $SrTiO_3$", *Phys. Rev. B* 13:271-286.

[4] Itoh, M., Wang, R., Inaguma, Y., Yamaguchi, T., Shan, Y. J., Nakamura, T. 1999. "Ferroelectricity Induced by Oxygen Isotope Exchange in Strontium Titanate Perovskite." *Phys. Rev. Lett.* 82:3540-3543.

[5] Lemanov, V. V. 2004. "Phase Transitions in Perovskite Solid Solutions with Incipient Ferroelectrics." *Ferroelectrics* 302:169-173.

[6] Vendik, O. G., Hollmann, E. K., Kozyrev, A. B., Prudan, A. M. 1999. "Ferroelectric Tuning of Planar and Bulk Microwave Devices." *J. Supercond.* 12:325-338.

[7] Tagantsev, A. K., Sherman, V. O., Astafiev, K. F., Venkatesh, J., Setter, N. 2003. "Ferroelectric Materials for Microwave Tunable Applications." *J. Electroceram.* 11:5-66.

[8] Lytle, F. W. 1964. "X-ray Diffractometry of Low-temperature Phase Transformations in Strontium Titanate." *J. Appl. Phys.* 35:2212-2215.

[9] Frederikse, H. P. R., Thurber, W. R., Hosler, W. R. 1964. "Electronic Transport in Strontium Titanate." *Phys. Rev*. 134:A442-A445.

[10] Schooley, J. F., Hosler, W. R., Cohen, M. L. 1964. "Superconductivity in Semiconducting $SrTiO_3$." *Phys. Rev. Lett.* 12:474-475.

[11] Koumoto, K., Wang, Y., Zhang, R., Kosuga, A., Funahashi, R. 2010. "Oxide Thermoelectric Materials: A Nanostructuring Approach." *Annu. Rev. Mater. Res*. 40:363-394.

[12] Yamaoka, N. "$SrTiO_3$-based Boundary-layer Capacitors." 1986. *Am. Ceram. Soc. Bull.* 65:1149-1152.

[13] Shen, H., Song, Y. W., Gu, H., Wang, P. C., Xi, Y. M. 2002. "A high-Permittivity $SrTiO_3$-based Grain Boundary Barrier Layer Capacitor Material Single-fired under Low Temperature." *Mater. Lett.* 56:802-805.

[14] Li, J. Y., Li, S. T., Alim, M. A. 2006. "The Effect of Reducing Atmosphere on the $SrTiO_3$ Based Varistor-capacitor Materials." *J. Mater. Sci.-Mater. El.* 17:503-508.

[15] Li, J. Y., Luo, S. H., Alim, M. A. 2006. "The Role of TiO_2 Powder on the $SrTiO_3$-based Synthesized Varistor Materials." *Mater. Lett.* 60:720-724.

[16] Johnson, K. D., Dravid, V. P. 1999. "Grain Boundary Barrier Breakdown in Niobium Donor Doped Strontium Titanate Using in situ Electron Holography." *Appl. Phys. Lett.* 74:621-623.

[17] Kingon, A. 2006. "Perovskites: Is the Ultimate Memory in Sight?" *Nat. Mater.* 5:251-252.

[18] Kotecki, D. E., Baniecki, J. D., Shen, H., Laibowitz, R. B., Saenger, K. L., Lian, J. J., Shaw, T. M., Athavale, S. D., Cabral, C., Duncombe, P. R., Gutsche, M., Kunkel, G., Park, Y. J., Wang, Y. Y., Wise, R. 1999. "$(Ba,Sr)TiO_3$ Dielectrics for Future Stacked-capacitor DRAM." *IBM J. Res. Dev.* 43:367-382.

[19] Eisenbeiser, K., Finder, J. M., Yu, Z., Ramdani, J., Curless, J. A., Hallmark, J. A., Droopad, R., Ooms, W. J., Salem, L., Bradshaw, S., Overgaard, C. D. 2000. "Field Effect Transistors with $SrTiO_3$ Gate Dielectric on Si." *Appl. Phys. Lett.* 76:1324-1326.

[20] Meyer, R., Waser, R. 2004. "Resistive Donor-doped $SrTiO_3$ Sensors: I. Basic Model for a Fast Sensor Response." *Sensor Actuat. B-Chem.* 101:335-345.

[21] Kolodiazhnyi, T., Petric, A. 2005. "The Applicability of Sr-deficient n-type $SrTiO_3$ for SOFC Anodes." *J. Electroceram.* 15:5-11.

[22] Last, J. T. 1957. "Infrared-absorption Studies on Barium Titanate and Related Materials." *Phys. Rev.* 105:1740-1750.

[23] Goldschmidt, V. M. 1927. *Geochemisce verterlungsgesetze der elemente*. Oslo: Norske Videnskap.

[24] Bhalla, A. S., Guo, R. Y., Roy, R. 2000. "The Perovskite Structure - a Review of its Role in Ceramic Science and Technology." *Mater. Res. Innov.* 4:3-26.

[25] Mitsui, T., Westphal, W. B. 1961. "Dielectric and X-ray Studies of $Ca_xBa_{1-x}TiO_3$ and $Ca_xSr_{1-x}TiO_3$." *Phys. Rev.* 124:1354-1359.

[26] Rimai, L., deMars, G. A. 1962. "Electron Paramagnetic Resonance of Trivalent Gadolinium Ions in Strontium and Barium Titanates." *Phys. Rev.* 127:702-710.

[27] Unoki, H., Sakudo, T. 1967. "Electron Spin Resonance of Fe^{3+} in $SrTiO_3$ with Special Reference to 110 K Phase Transition." *J. Phys. Soc. Jpn.* 23:546-552.

[28] Witek, S., Smyth, D. M., Pickup, H. 1984. "Variability of the Sr/Ti Ratio in $SrTiO_3$." *J. Am. Ceram. Soc.* 67:372-375.

[29] Han, Y. H., Harmer, M. P., Hu, Y. H., Smyth, D. M. 1985. "A^{2+}/Ti Nonstoichiometry in Alkaline Earth Titanates, $ATiO_3$." In *Transport in Nonstoichiometric Compounds*, edited by G. Simkovich and V. S. Stubican. 73-75. New York: Plenun Press.

[30] Balachandran, U., Eror, N. G. 1982. "On the Defect Structure of Strontium-titanate with Excess SrO." *J. Mater. Sci.* 17:2133-2140.

[31] Eror, N. G., Balachandran, U. 1982. "Electrical-conductivity in Strontium Titanate with Nonideal Cationic Ratio." *J. Solid. State Chem.* 42:227-241.

[32] Amaral, L., Senos, A. M. R., Vilarinho, P. M. 2009. "Sintering Kinetic Studies in Nonstoichiometric Strontium Titanate Ceramics." *Mater. Res. Bull.* 44:263-270.

[33] Akhtar, M. J., Akhtar, Z. U. N., Jackson, R. A., Catlow, C. R. A. 1995. "Computer-simulation Studies of Strontium Titanate." *J. Am. Ceram. Soc.* 78:421-428.

[34] Kim, M., Duscher, G., Browning, N. D., Sohlberg, K., Pantelides, S. T., Pennycook, S. J. 2001. "Nonstoichiometry and the Electrical Activity of Grain Boundaries in $SrTiO_3$." *Phys. Rev. Lett.* 86:4056-4059.

[35] Chung, S. Y., Yoon, D. Y., Kang, S. J. L. 2002. "Effects of Donor Concentration and Oxygen Partial Pressure on Interface Morphology and Grain Growth Behavior in $SrTiO_3$." *Acta Mater.* 50:3361-3371.

[36] Meyer, R., Waser, R., Helmbold, J., Borchardt, G. 2002. "Cationic Surface Segregation in Donor-doped $SrTiO_3$ under Oxidizing Conditions." *J. Electroceram.* 9:101-110.

[37] Moos, R., Hardtl, K. H. 1997. “Defect Chemistry of Donor-doped and Undoped Strontium Titanate Ceramics between 1000° and 1400°C.”, *J. Am. Ceram. Soc.* 80:2549-2562.

[38] Ianculescu, A., Brăileanu A., Voicu, G. 2007. “Synthesis, Microstructure and Dielectric Properties of Antimony-doped Strontium Titanate Ceramics.” *J. Eur. Ceram. Soc.* 27:1123-1127.

[39] You, I. K., Byun, J. D., Kim, Y. H. 1996. “The Microstructure and Electrical Conductivity of WO_3-doped $SrTiO_3$ Ceramics.” *Solid State Ion.* 83:159-165.

[40] Suzuki, T., Nishi, Y., Fujimoto, M. 2000. “Defect Structure in Homoepitaxial Non-stoichiometric Strontium Titanate Thin Films.” *Philos. Mag. A* 80:621-637.

[41] Balachandran, U., Eror, N. G. 1982. “Oxygen Nonstoichiometry of Tantalum-doped $SrTiO_3$.” *J. Less-Common Met.* 85:11-19.

[42] Bäurer, M., Kungl, H., Hoffmann, M. J. 2009. “Influence of Sr/Ti stoichiometry on the Densification Behavior of Strontium Titanate.” *J. Am. Ceram. Soc.* 92:601-606.

[43] Wang, D. Y., Umeya, K. 1990. “Depletion Layer Dielectric Properties of Positive Temperature Coefficient of Resistance Barium Titanate.” *J. Am. Ceram. Soc.* 73:1574-1581.

[44] Wilcox, N., Ravikumar, V., Rodrigues, R. P., Dravid, V. P., Vollman, M., Waser, R., Soni, K. K., Adriaens, A. G. 1995. “Investigation of Grain-boundary Segregation in Acceptor and Donor-doped Strontium Titanate.” *Solid State Ion.* 75:127-136.

[45] Chiang, Y. M., Takagi, T. 1990. “Grain Boundary Chemistry of Barium Titanate and Strontium Titanate: I. High-temperature Equilibrium Space-charge.” *J. Am. Ceram. Soc.* 73:3278-3285.

[46] Waser, R., Hagenbeck, R. 2000. “Grain Boundaries in Dielectric and Mixed Conducting Ceramics.” *Acta Mater.* 48:797-825.

[47] Chiang, Y. M., Takagi, T. 1990. “Grain-boundary Chemistry of Barium-titanate and Strontium-titanate: II. Origin of Electrical Barriers in Positive-temperature-Coefficient Thermistors.” *J. Am. Ceram. Soc.* 73:3286-3291.

[48] Waser, R. 1995. "Electronic-properties of Grain-boundaries in $SrTiO_3$ and $BaTiO_3$ Ceramics." *Solid State Ion.* 75:89-99.

[49] Browning, N. D., Buban, J. P., Moltaji, H. O., Pennycook, S. J., Duscher, G., Johnson, K. D., Rodrigues, R. P., Dravid, V. P. 1999. "The Influence of Atomic Structure on the Formation of Electrical Barriers at Grain Boundaries in $SrTiO_3$", *Appl. Phys. Lett.* 74:2638-2640.

[50] Klie, R. F., Browning, N. D. 2000. "Atomic Scale Characterization of Oxygen Vacancy Segregation at $SrTiO_3$ Grain Boundaries." *Appl. Phys. Lett.* 77:3737-3739.

[51] Bäurer, M., Shih, S. J., Bishop, C., Harmer, M. P., Cockayne, D., Hoffmann, M. J. 2010. "Abnormal Grain Growth in Undoped Strontium and Barium Titanate." *Acta Mater.* 58:290-300.

[52] Bäurer, M., Stormer, H., Gerthsen, D., Hoffmann, M. J. 2010. "Linking Grain Boundaries and Grain Growth in Ceramics." *Adv. Eng. Mater.* 12:1230-1234.

[53] von Alfthan, S., Benedek, N. A., Chen, L., Chua, A., Cockayne, D., Dudeck, K. J., Elsasser, C., Finnis, M. W., Koch, C. T., Rahmati, B., Ruhle, M., Shih, S. J., Sutton, A. P. 2010. "The Structure of Grain Boundaries in Strontium Titanate: Theory, Simulation and Electron Microscopy." *Annu. Rev. Mater. Res.* 40:557-599.

[54] Rheinheimer, W., Hoffmann, M. J. 2016. "Grain Growth in Perovskites: What is the Impact of Boundary Transitions?" *Curr. Opin. Solid State Mater. Sci*. 20:286-298.

[55] Rohrer, G. S. 2005. "Influence of Interface Anysotropy on Grain Growth and Coarsening." *Annu. Rev. Mater. Res.* 35:99-126.

[56] Sano, T., Rohrer, G. S. 2007. "Experimental Evidence for the Development of Bimodal Grain Size Distributions by the Nucleation-limited Coarsening Mechanism." *J. Am. Ceram. Soc.* 90:211-216.

[57] Chung, S. Y., Kang, S. J. L. 2000. "Effect of Dislocations on Grain Growth in Strontium Titanate." *J. Am. Ceram. Soc.* 83:2828-2832.

[58] Levin, E. M., Robbins, C. R., McMurdie, H. F. 1964. *Phase diagrams for ceramists*. Columbus: The American Ceramic Society.

[59] Chung, S. Y., Kang, S. J. L. 2003. "Intergranular Amorphous Films and Dislocations-promoted Grain Growth in $SrTiO_3$." *Acta Mater.* 51:2345-2354.

[60] Lee, S. B., Sigle, W., Kurtz, W., Ruhle, M. 2003. "Temperature Dependence of Faceting in Σ5(310)[001] Grain Boundary of $SrTiO_3$." *Acta Mater.* 51:975-981.

[61] Lee, S. B., Sigle, W., Ruhle, M. 2003. "Faceting Behavior of an Asymmetric $SrTiO_3$ Σ5[001] Tilt Grain Boundary Close to Its Defaceting Transition." *Acta Mater.* 51:4583-4588.

[62] Lee, S. B., Lee, J. H., Cho, P. S., Kim, D. Y., Sigle, W., Phillipp, F. 2007. "High-temperature Resistance Anomaly at a Strontium Titanate Grain Boundary and its Correlation with the Grain-boundary Faceting-defaceting Transition", *Adv. Mater.* 19:391-395.

[63] Peng, C. J., Chiang, Y. M. 1990. "Grain-Growth in Donor-Doped $SrTiO_3$." *J. Mater. Res.* 5:1237-1245.

[64] Chen, J. S., Young, R. J., Wu, T. B. 1987. "Densification and Microstructural Development of $SrTiO_3$ sintered with V_2O_5." *J. Am. Ceram. Soc.* 70:C260-C264.

[65] Amaral, L., Senos, A. M. R., Vilarinho, P. M. 2008. "Nonstoichiometry Effects in $SrTiO_3$ Ceramics Assessed by Transmission Electron Microscopy." *Microsc. Microanal.* 14**(**S3):5-6.

[66] Tkach, A., Vilarinho, P. M., Senos, A. M. R., Kholkin, A. L. 2005. "Effect of Nonstoichiometry on the Microstructure and Dielectric Properties of Strontium Titanate Ceramics." *J. Eur. Ceram. Soc.* 25:2769-2772.

[67] Bae, C., Park, J. G., Kim, Y. H., Jeon, H. 1998. "Abnormal Grain Growth of Niobium-doped Strontium Titanate Ceramics." *J. Am. Ceram. Soc.* 81:3005-3009.

[68] Shih, S. J., Lozano-Perez, S., Cockayne, D. J. H. 2010. "Investigation of Grain Boundaries for Abnormal Grain Growth in Polycrystalline $SrTiO_3$." *J. Mater. Res.* 25:260-265.

[69] Dillon, S. J., Tang, M., Carter, W. C., Harmer, M. P. 2007. "Complexion: A New Concept for Kinetic Engineering in Materials Science." *Acta Mater.* 55:6208-6218.

[70] Dillon, S. J., Harmer, M. P. 2008. "Relating Grain Boundary Complexion to Grain Boundary Kinetics II: Silica-doped Alumina." *J. Am. Ceram. Soc.* 91:2314-2320.

[71] Dillon, S. J., Harmer, M. P. 2008. "Relating Grain-boundary Complexion to Grain-boundary Kinetics I: Calcia-doped Alumina." *J. Am. Ceram. Soc.* 91:2304-2313.

[72] Bäurer, M., Weygand, D., Gumbsch, P., Hoffmann, M. J. 2009. "Grain Growth Anomaly in Strontium Titanate." *Scripta Mater.* 61:584-587.

[73] Amaral, L., Fernandes, M., Reaney, I. M., Harmer, M. P., Senos, A. M. R., Vilarinho, P. M. 2013. "Grain Growth Anomaly and Dielectric Response in Ti-rich Strontium Titanate Ceramics." *J. Phys. Chem. C* 117:24787-24795.

[74] Tkach, A., Amaral, L., Vilarinho, P. M., Senos, A. M. R. 2018. "Oxygen Vacancies as a Link between the Grain Growth and Grain Boundary Conductivity Anomalies in Titanium-rich Strontium Titanate." *J. Eur. Ceram. Soc.* 38:2547-2552.

[75] Amaral, L., Tkach, A., Reaney, I. M., Vilarinho, P. M., Senos, A. M. R. 2019. "New Insights into the Effect of Nonstoichiometry on the Electric Response of Strontium Titanate Ceramics." *J. Phys. Chem. C*, 123:710-718.

[76] Burke, J. E., Turnbull, D. 1952. "Recrystallization and Grain Growth." *Progr. Metal Phys.* 3:220-292.

[77] Kang, S. J. L. 2005. *Sintering: Densification, Grain Growth and Microstructure*. Oxford: Elsevier.

[78] Dillon, S. J., Behera, S. K., Harmer, M. P. 2008. "An Experimentally Quantifiable Solute Drag Factor." *Acta Mater.* 56:1374-1379.